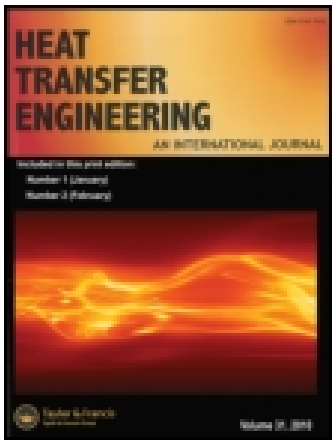

Heat Transfer Engineering
Publication details, including instructions for authors and subscription information:
http://www.tandfonline.com/loi/uhte20

Numerical Simulation and Experimental Analysis of a Modular Storage System for Direct Steam Generation

Andreas Stückle [a] , Doerte Laing [a] & Hans Müller-Steinhagen [b]
[a] Institute of Technical Thermodynamics, German Aerospace Center (DLR) , Stuttgart , Germany
[b] Technische Universität Dresden , Dresden , Germany
Accepted author version posted online: 29 Jul 2013.Published online: 17 Dec 2013.

To cite this article: Andreas Stückle , Doerte Laing & Hans Müller-Steinhagen (2014) Numerical Simulation and Experimental Analysis of a Modular Storage System for Direct Steam Generation, Heat Transfer Engineering, 35:9, 812-821, DOI: 10.1080/01457632.2013.828556

To link to this article: http://dx.doi.org/10.1080/01457632.2013.828556

Heat Transfer Engineering, 35(9):812–821, 2014

ISSN: 0145-7632 print / 1521-0537 online
DOI: 10.1080/01457632.2013.828556

Taylor & Francis
Taylor & Francis Group

Numerical Simulation and Experimental Analysis of a Modular Storage System for Direct Steam Generation

ANDREAS STÜCKLE,[1] DOERTE LAING,[1] and HANS MÜLLER-STEINHAGEN[2]

[1]Institute of Technical Thermodynamics, German Aerospace Center (DLR), Stuttgart, Germany
[2]Technische Universität Dresden, Dresden, Germany

Thermal energy storage is a key technology for the commercialization of solar thermal power plants. This paper gives an overview of a coupled system comprised of concrete regenerators and latent heat storages for direct steam generation, as developed by the German Aerospace Center. Methodologies for an effective transient numerical description of the heat conduction processes inside the single modules and in the whole storage system are presented and their validity is proven by experiments. The presented process has a nominal system pressure of 105.6/80.0 bar for charging/discharging; the corresponding boiling temperatures are 315/295°C. As storage material of the latent heat storage, sodium nitrate with a melting point of 305°C is applied. With the presented models, a prediction of the storage system's temperatures, capacities, and effectiveness is possible. As a result, the design of a 1000-MWh_{th} storage system is presented.

INTRODUCTION

Concentrated solar power (CSP) plants use mirrors to focus solar radiation on receivers that convert it into heat. This thermal energy is then used to produce electricity, for example, in an almost conventional steam turbine power block. Parabolic trough power plants using synthetic oil as the heat transfer fluid (HTF) are currently the most frequently applied systems for commercial CSP power generation. To improve their cost-effectiveness, one focus of research is the substitution of synthetic oil by water/steam as the HTF in the solar field, which is the so-called direct steam generation (DSG). The HTF is preheated, evaporated, and superheated directly in the receiver tubes of the parabolic troughs. This concept has been running since the 1990s. It was part of the project Solar Thermal Electricity in the Mediterranean (STEM) [1–3].

One major advantage of solar thermal power plants over photovoltaic systems is the possibility for storing the collected solar energy in thermal energy storage. This allows CSP plants to be designed with higher annual capacity factors, to extend electricity production into periods with low solar radiation and after sunset, to produce electricity according to demand, and to support grid reliability. This leads to an increased profitability, as the CSP plant is able to generate electricity when the market demand is at peak and to offer maximum electric power [4].

In a CSP plant, direct steam generation is not only a challenge for the solar field, but also the storage system needs to be adapted to the two-phase fluid water/steam. For evaporating the water, large amounts of heat have to be provided at a constant temperature level. A storage system using only sensible heat storage is not suited to this purpose. In contrast, latent heat storage can absorb/supply large amounts of heat within a narrow temperature interval. It is based on phase-change materials (PCM) that can undergo phase transitions in the desired temperature range, for example, from solid to liquid state [5]. Therefore, for an efficient storage solution for direct steam generation, a combination of latent and sensible heat storage technologies needs to be applied, presenting a substantial challenge to system operation.

Address correspondence to Doerte Laing, Institute of Technical Thermodynamics, Deutsches Zentrum für Luft- und Raumfahrt e.V., Pfaffenwaldring 38-40, 70569 Stuttgart, Germany. E-mail: doerte.laing@dlr.de

State of the Art: Thermal Energy Storage in Solar Thermal Power Plants for Direct Steam Generation

An example of a DSG solar power plant including a storage system is the solar power tower PS 10 in Spain. Solar radiation is focused by heliostats on the tower's receiver. The receiver produces saturated steam to run a turbine. Additionally, the saturated steam can be stored in a Ruths storage device [6].

A Ruths storage device is a vessel that stores water in both the liquid and vapor phases. When charging with saturated steam, pressure increases and with it the boiling point. Therefore, condensate fills the vessel. A Ruths storage device can be filled up to 95% with the liquid phase [7]. Disadvantageous are the limited maximum pressure of about 40 bar and the high specific costs. Higher pressures would require strong walls, which result in high material costs. Another disadvantage is the sliding pressure, increasing when charging and decreasing when discharging [8].

Therefore, this system is not suitable for the intended application.

New Concept Thermal Energy Storage System for Direct Steam Generation

For the special requirements of CSP plants with direct steam generation, a modular storage system combining sensible and latent heat storage was developed by German Aerospace Center (DLR) in cooperation with Ed. Züblin AG within the project ITES which was partly funded by the German Federal Ministry for the Environment, Nature Conservation and Nuclear Safety [9]. The heat required for evaporating the water is stored in the latent heat storage, while sensible concrete storage units store the thermal energy for preheating and superheating (see Figure 1). The concrete units are regenerator-type storage units, which increase their temperature during charging and decrease it during discharging. The latent heat storage units use the heat of fusion of the phase-change storage material and therefore keep an almost constant temperature during charging and discharging. The individual modules are labeled preheater, evaporator, and superheater modules, according to their function during the discharging process.

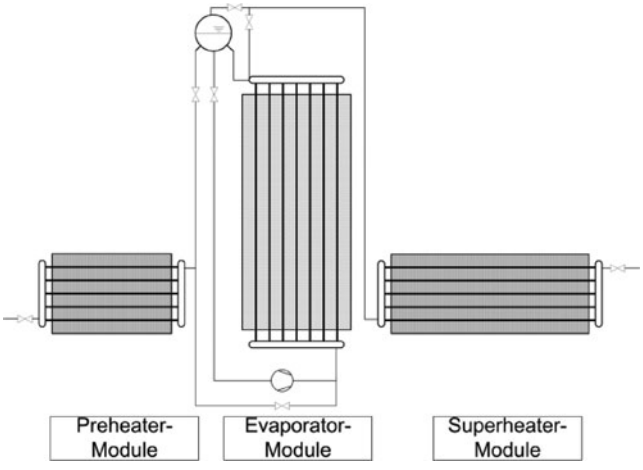

Figure 1 Modular storage system for direct steam generation.

The current status is shown by a pilot plant with a PCM storage unit and concrete regenerator operated by DLR in Carboneras, Spain. Commissioning was successful and operational reliability has been demonstrated [10]. Parallel to the system demonstration, suitable system models to describe the systems performance were developed. The aim is to predict temperatures, pressures, mass flow rates, capacity, heat losses, and the efficiency in a larger scale system.

In the following, the system models of the different modules are described and validated by experiments. As the overall result, the detailed design of a 1000-MWh_{th} system is proposed.

BOUNDARY CONDITIONS

For the following numerical investigations, system parameters were adapted to a steam cycle operating at 100 bar, corresponding to a saturation temperature of 311°C. In a first step, sodium nitrate was identified as a suitable phase change material in terms of this temperature range. Sodium nitrate has a melting temperature of 305°C (see Table 1). For charging and discharging the latent heat storage, a driving temperature difference of 10 K was selected. This results in a system pressure of the water/steam cycle of 105.6 bar (315°C saturation temperature) for charging and 80 bar (295°C saturation temperature) for discharging. The system parameters for the whole plant are described by Birnbaum et al. [3] using 400°C/110 bar as inlet parameters for the superheater module during charging and a feed-water temperature (FWT) of 260°C at full load as the inlet parameter for the preheater module during discharging.

The superheater concrete regenerator cools down the incoming superheated steam when charging. The evaporator PCM module condenses the slightly superheated incoming steam at 105.6 bar and 315°C, which is 10 K above the PCM's melting temperature. The condensate is then cooled down by the preheater concrete regenerator. For discharging, this process is reversed. The pressure is lowered to 80.0 bar to generate a temperature difference between the PCM storage and the boiling temperature of 10 K. The feed water is preheated in the preheater regenerator, then evaporated in the PCM module, and the generated saturated steam is superheated in the superheater regenerator.

Table 1 Thermophysical properties of the used $NaNO_3$

Property	Solid	Liquid	Unit
Thermal conductivity	0.6	0.55	W/(m-K)
Density	2110	1910	kg/m^3
Specific heat capacity	1500	1700	J/(kg-K)
Enthalpy of fusion	175,000		J/kg
Fusion point	305		°C

THERMAL MODELING

An effective transient model with a short calculation time is required in order to allow a fast simulation of the system during a real time period of days or even months. Furthermore, the model must be fully parameterized to allow quick iterative dimensioning of single modules and whole storage systems. Therefore, commercial numerical tools such as computational fluid dynamics (CFD) or the finite-element method (FEM) are inappropriate. For the present work, the modules' models were created in Modelica [11, 12]. As user interface, Dymola is used.

The local heat flow in the concrete and PCM modules is modeled as hollow cylinder elements. The respective partial differential equations, described in the following, are solved by using the central second-order finite-element method. The concrete modules are discretized only in axial and the PCM modules both in axial and radial directions of the hollow cylinder.

To solve the resulting differential algebraic equations (DAEs) the numerical solver ESDIRK 34a [13] is used. This solver is a 4th one-step procedure with variable time steps for stiff systems. The advantage of this method is that the discontinuities occurring e.g. when shifting the storage models from charging to discharging mode are easily solved and the variable time steps allow a quick overall solution.

Modeling of the Concrete Modules

As depicted in Figure 2, the regenerator is characterized by a tube bank that is surrounded by the storage material. This storage material is a custom-made high-temperature concrete [14]. The average thermophysical properties of the concrete regenerator are specific heat capacity of 955 J/(kg-K) and thermal conductivity of 1.3 W/(m-K). To attain a simplified model, one of the tubes is abstracted with the assumption that all tubes carry the same mass flow rate. The abstracted tube is assumed to be a hollow cylinder, and is then multiplied by the total number of tubes to model the volume of the entire regenerator. Equation (1) is the energy balance of a cylindrical flow element of the tube.

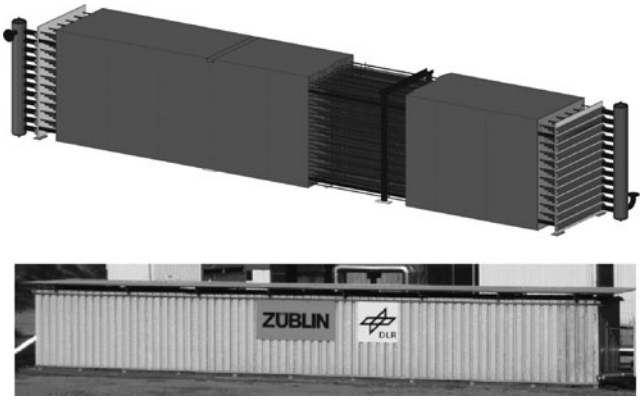

Figure 2 Concrete regenerator in the water/steam test loop of the Litoral power plant of Endesa in Carboneras, Spain.

$$\rho_f c_f \frac{\partial T_f}{\partial t} + \rho_f c_f \frac{\dot{V}_f}{A_{c,f}} \frac{\partial T_f}{\partial x} = \lambda_{fx} \frac{\partial^2 T_f}{\partial x^2} + \lambda_{fr} \left[\frac{\partial^2 T_f}{\partial r_f^2} + \frac{1}{r_f} \frac{\partial T_f}{\partial r_f} \right] \quad (1)$$

The first left-hand term is the thermal power density of the element, and the second term is the thermal power density change caused by the flow through the element. The right-hand terms are the heat flow densities in axial and radial direction. The fluid flow is assumed to have no heat conduction in the axial and the radial directions. The assumption of constant fluid temperature in radial direction is due to the large ratio of tube length to diameter. The axial heat conduction inside the fluid is neglected because of the fluid velocity and low thermal conductivity. Therefore, Eq. (1) can be reduced to:

$$\rho_f c_f \frac{\partial T_f}{\partial t} + \rho_f c_f \frac{\dot{V}_f}{A_{c,f}} \frac{\partial T_f}{\partial x} = 0 \quad (2)$$

Equation (2) is written for an axial element of length Δx, including the heat flow rate between the fluid and the inner surface of the tube:

$$\alpha \pi 2 r_i (T_s - T_f) + \dot{m}_f c_f T_f|_x = \dot{m}_f c_f T_f|_{x+1} + A_{c,f} \Delta x \rho_f c_f \frac{\partial T_f}{\partial t} \quad (3)$$

The first term on the left side of the equation is the heat flow rate governed by a convective heat transfer between the fluid and the inner surface element of the tube. The convective heat transfer coefficient was determined by a dimensionless average Nusselt correlation for a single-phase fluid flow with the assumption of a constant wall temperature [15]. The second left-hand term is the heat flow rate entering the balance element at the axial coordinate x. The first right-side term is the heat flow rate leaving the balance element and the second term describes the time-dependent enthalpy change inside the balance element. The temperatures without an index for the coordinate are always the mean values from the temperatures at the coordinates x and $x + 1$.

Due to the requirement for a fast numerical solution, an approach to simplify the two-dimensional (2D) transient heat conduction problem inside the hollow cylindrical heat storage mass was sought. Schmidt and Willmott [16] describe a method, originally developed by Hausen [17], where the heat transfer coefficient between fluid and storage is adapted in order to account for the radial heat conduction inside the hollow cylinder. With this approach, the radial dimension of the hollow cylinder is treated as a lumped system. Heat conduction in axial direction is neglected due to the large ratio of the hollow cylinder length to radius.

In Eq. (4), the first left-side term is the change of lumped capacity of the regenerator, the second term is the regenerator's

heat losses to the environment, and the right-hand-side term is the transferred heat between the HTF and the storage material:

$$\rho_s c_s V_s \frac{\partial T_s}{\partial t} + \alpha_L A_L (T_s - T_{amb}) = \alpha_H A (T_f - T_s) \qquad (4)$$

This equation is set up and solved for the several axial elements.

$$\pi (r_o - r_i)^2 \Delta x \rho_s c_s \left. \frac{\partial T_s}{\partial t} \right|_x$$

$$+ \alpha_L \pi 2 r_o \Delta x (T_s - T_{amb})|_x = \alpha_H \pi 2 r_i \Delta x (T_s - T_f)|_x \qquad (5)$$

In the present work, the second left-side term, which describes the heat losses at the outer diameter of a cylinder, is replaced by a temperature-dependent function describing the overall heat loss rate. The function was determined in an experiment according to the method of Schack [18] for the overall regenerator, accounting for both radiation and convection:

$$\dot{Q}_L = K'_L \cdot (T_S - T_{amb})^{1+m} \qquad (6)$$

with the coefficient $K'_L = 9.35$ W/K and the exponent m = 0.201. Before adopting Eq. (6) as second term of Eq. (5), the overall heat loss rate is divided by the number of parallel tubes and discrete axial elements.

The adapted heat transfer coefficient α_H is a combination of the heat transfer coefficient for forced convection inside a tube [15] and the heat conduction inside the storage material,

$$\frac{1}{\alpha_H} = \frac{1}{\alpha} + \frac{\Delta}{\lambda} \qquad (7)$$

with Δ for the hollow cylinder (from [13]):

$$\Delta = \frac{r_i}{2\left(r_o^2 - r_i^2\right)} \frac{2 r_o^4}{r_o^2 - r_i^2} \ln\left(\frac{r_o}{r_i}\right) - 2 r_o^2 + r_i^2 \qquad (8)$$

Equation (3) is coupled with Eq. (5) by the term describing the transferred heat.

The described model was validated at a test facility with synthetic oil as the HTF, by matching measured and calculated temperature curves of periodic repetitive cycles [19]. This allowed more accurate measurements than the also available water/steam test facility, as the cycle repetition was continuously and automatically driven. The difference between experimental and calculated results was within the accuracy of the measurements.

Modeling of the PCM Modules

The PCM storage shown in Figure 3 uses a tube bank with thin radial fins (see Figure 4) to enhance the heat flow, which is constrained by the poor thermal conductivity of about 0.55 W/(m-K) of the PCM sodium nitrate ($NaNO_3$). To describe the heat flow in the tube, fins, and PCM, a detailed model was developed [20]. The disadvantage of this detailed model is its long calculation time. Therefore, it is only used to determine the thermal conductivity of the simplified system model, which consists of a hollow cylindrical geometry of a model storage material that is composed of steel tubes, aluminium fins and the PCM $NaNO_3$. The system model of the PCM storage is a hollow cylinder with transient heat conduction in radial and axial direction, which can be described with the following equation:

Figure 3 PCM storage in the water/steam test loop at the Litoral power plant of Endesa in Carboneras, Spain.

$$\rho_s c_s \frac{\partial T_s}{\partial t} = \lambda_{sx} \frac{\partial^2 T_s}{\partial x^2} + \lambda_{sr} \left[\frac{\partial^2 T_s}{\partial r_s^2} + \frac{1}{r_s} \frac{\partial T_s}{\partial r_s} \right] \qquad (9)$$

Figure 4 Finned tube of the PCM storage.

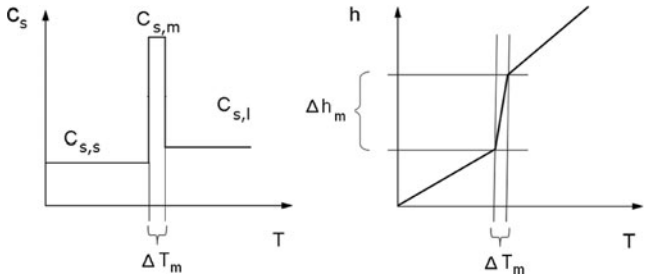

Figure 5 PCM physical property model.

Rotational symmetry is assumed due to the vertical alignment of the tube register. When describing horizontal tubes surrounded by PCM, this assumption will probably not be fully valid, as density differences within the liquid phase of the PCM can lead to convection that enhances melting around the tube and results in an asymmetric melt front [21]. The vertical installation is advantageous for several reasons. Thermal expansion of various components is easier to handle, the condensate produced in the tube during charging can easily drain off, the forced circulation evaporation process is supported by the developing density reduction from the lower to the upper end of the tube, and the two-phase heat transfer mechanisms on the fluid side of this storage are rotationally symmetric. Inside a horizontal tube, an asymmetric channel flow would be expected.

The specific heat capacity of the storage material c_s in Eq. (9) is formulated as a temperature-dependent function to represent the enthalpy of fusion. In Modelica, an if-clause is used which defines the assumed values of the specific heat capacity of $NaNO_3$ as shown in Table 1 and in Figure 5.

In order to improve the numerical stability the model assumes a temperature range ΔT_m from 304.5 to 305.5°C instead of a constant-temperature melting process. According to the qualitative distributions of the specific heat capacity and of the specific enthalpy of the PCM depicted in Figure 5, the enthalpy of fusion is described by the following equation:

$$c_m = \frac{\Delta h_m}{\Delta T_m} = 175{,}000 \text{ J/(kg-K)} \tag{10}$$

The thermal conductivity of the model material in the axial direction is that of the PCM. The radial conductivity is determined by a detailed model that accounts for a detailed 2D heat flow in the tube, fins, and PCM. As already described, the detailed model is not suitable for system calculations due to its long calculation times. Therefore, a simulation environment was built to match the detailed model with the system model. In this case, both models are adiabatic and receive periodically repeating boundary conditions, which means a temperature of 315°C on the inner surface of the tube when charging and 295°C when discharging. Although the detailed model parameters such as fin properties are set as in the experiment, the radial thermal conductivity of the system model is iteratively adjusted as melting and freezing take the same time in both models (see Figure 6). At that point, the curves of the transferred heat flow rates are almost identical (see Figure 7). For the PCM storage in this work,

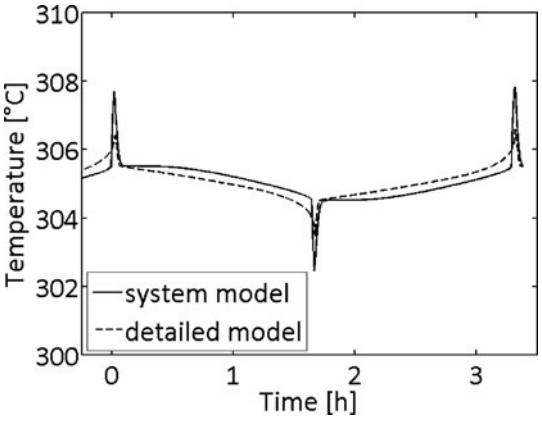

Figure 6 PCM temperature at the outer diameter of the calculation domain.

an effective radial thermal conductivity of the model storage material of 13.5 W/(m-K) was determined.

Modeling of the Filmwise Condensation During Charging

When charging the PCM storage, saturated or slightly superheated steam enters the tube register from the top. The experimental setup (see Figure 8) uses a condensate drain under the bottom end to separate the liquid from the vapor phase. Assuming continuity, the feed steam is equal to the generated condensate. To model the heat transfer coefficient during charging, a correlation from Numrich and Müller [22] is used. Therefore, local heat transfer coefficients without vapor flow are calculated for the axial segments accounting for the waviness of the condensate film and temperature-dependent physical properties. The model combines laminar and turbulent flow as follows:

$$Nu_x = f_\eta \sqrt{(f_{well} Nu_{x,l})^2 + Nu_{x,t}^2} \tag{11}$$

$$\alpha_x = \frac{Nu_x \lambda_F}{\sqrt[3]{\frac{\upsilon_F^2}{g}}} \tag{12}$$

With this approach, the maximum transferable heat flow rate is attained. Operating the storage module at maximum power

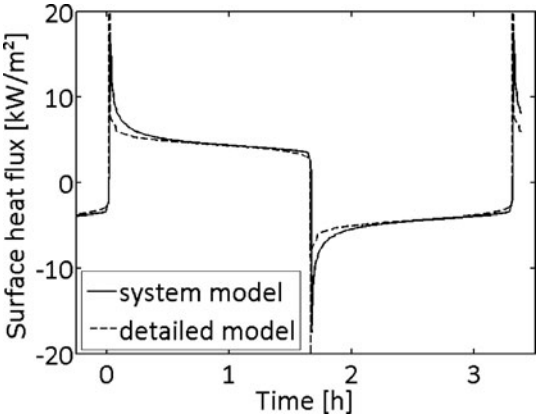

Figure 7 Detail PCM vs. system PCM model: transmitted heat flux.

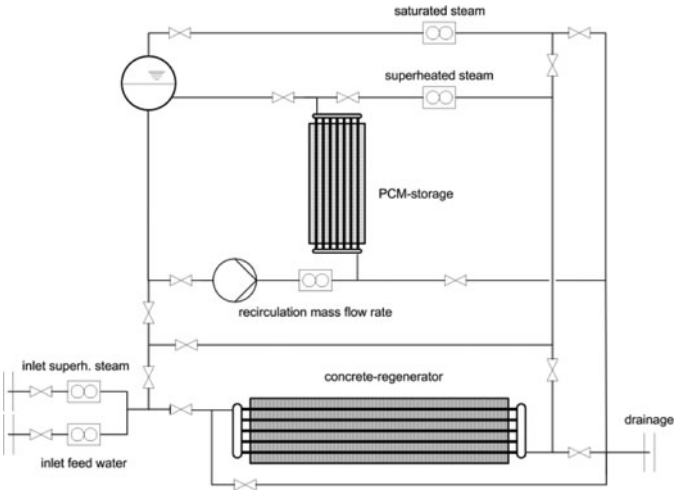

Figure 8 Simplified experimental set up of the DSG storage system with the position of the mass flow rate sensors.

Table 2 Parameters of PCM storage and concrete regenerator

Parameter	PCM module	Concrete module	Unit
Length	0.99	12.36	m
Width	1.39	1.35	m
Height	6.00	1.32	m
Number of tubes	152	144	—
Tube pitch	134	100 × 200	mm
Tube size	21.3 × 3.2	21.3 × 3.2	mm
Total volume	8.098	21.720	m^3
Mass of storage material	13.635	50.164	t
Mass of aluminum fins	2.150	—	t
Mass of steel	1.303	4.780	t
Total mass	17.088	54.944	t
Average density	2110	2530	kg/m^3
Heat transfer surface	42.690	82.157	m^2
Mineral rock wool	0.3	0.3	m
Number of nodes for calculation (axial/radial)	12 / 25	25	—

results in high rates at the beginning and quickly decreasing values with continuing discharging. For technical applications, an almost constant process is advantageous. For the case when the storage is not operated at its physical limit, the model calculates the transferred heat from the energy balance. That means that only the enthalpy flow rate entering the module can be transferred. In this case, the entire heat flow rate is evenly distributed along the axial elements. That is why the model is able to describe both maximum and partial load operation.

Modeling of the Evaporation

The module is discharged by forced circulation. Therefore, the system is equipped with a recirculation pump and a steam drum to separate the vapour from the liquid phase (see Figures 1, 3, and 8). Its fill level is used to control the inflow of feed water. Forced circulation with upward flow is used to adjust steady state conditions and equal flow conditions in all tubes. Due to the intended low steam quality, effects such as hydraulic shocks or different flow conditions in particular tubes are avoided. To describe the heat transfer, convective flow boiling is assumed. Baehr and Stephan [23] suggest an empirical approach. Bulk boiling (α_B) and a convective flow heat transfer coefficients (α_C) are calculated for the axial elements. According to Chen [24], suppression (S) and enhancement (F) factors are calculated, whereas the enhancement factor is determined using a Martinelli parameter.

$$\alpha = S\alpha_B + F\alpha_C \tag{13}$$

COMPARISON OF EXPERIMENTAL AND SIMULATED RESULTS

A simplified schematic of the experimental setup is shown in Figure 8. The test facility is supplied with steam and water by the coal-fired power plant Litoral of the energy supplier ENDESA in Carboneras, Spain. The modules can be supplied with the desired boundary conditions by mixing water and superheated stream. When charging, the set-point system pressure is 105.6 bar, whereas the boiling point is 315°C, so that the temperature difference between fluid and the melting point of the PCM $NaNO_3$ is 10 K and allows an adequate heat transfer. In analogy, when discharging, the system pressure is 80.0 bar with a boiling point of 295°C. The most important PCM storage and concrete regenerator parameters are given in Table 2. During the experiment, all relevant measurements are recorded in intervals of 60 s. The models use the measured inlet conditions as input boundary conditions.

The accuracy of the measured mass flow rates in the described experiments is better than ±6% of 1 kg/s, which is 0.06 kg/s. However, since the flow control valves of the test facility are not 100% leak-proof when closed, marginal leakage may occur. Therefore, a reliable error analysis for the measured mass flow values was not possible.

Concrete Module

The concrete module as shown in Figures 2 and 8 is charged and discharged with superheated steam (for physical properties as well as the number of finite elements used see Table 2). Due to the unsteady-state operation of the test facility, the regenerator cools down overnight, when the facility is shut down. To match the experimental results with the calculation results, the regenerator model's start values for the storage material temperature have to be initialized with the experimental values. Therefore, temperatures measured inside the storage materials with thermocouples are used to interpolate an initial temperature curve as shown in Figure 9. The increased heat losses at the end walls are accounted for. Starting with these conditions, the results of the matching of experiment and simulation is depicted in Figure 10. The measured and calculated fluid temperatures (monitored by

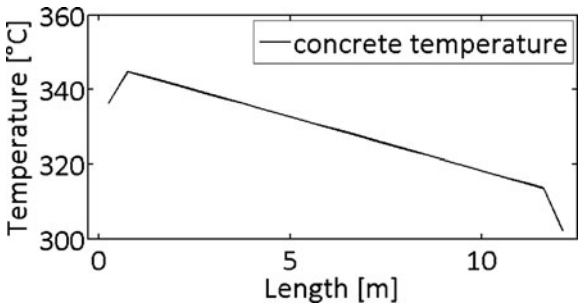

Figure 9 Initial temperature of the concrete regenerator.

PT100 sensors) at the inlet and outlet of the regenerators are called hot end (HE) and cold end (CE). In general, measured and calculated outlet temperatures are almost equal. Major deviations are only visible at the beginning of the cycles. This is due to unconsidered heat losses and the capacities of the fittings and piping of the test facility. During the first 20 min of charging, a constant outlet temperature is measured, which is due to at least partial condensation. When starting the experiment, the piping is cooled down due to the previous standstill period. Once the experimental setup has reached its operating temperature, measured and calculated curves are almost identical. After shifting to the discharging mode, the calculated outlet temperature is clearly higher than that calculated value for about 20 min. This is again caused by ignoring the heat capacities of piping and fittings. The predicted mass flow rate boundary condition is similar to the experimentally determined values (see Figure 10). Eventual fluctuations have no influence on the transient model.

PCM Module

The PCM storage shown in Figures 3 and 8 is charged with slightly superheated steam and discharged by generating saturated steam (for physical properties as well as geometric data see Table 2). To have defined initial parameters in the experiments, the PCM storage was heated to an almost constant temperature

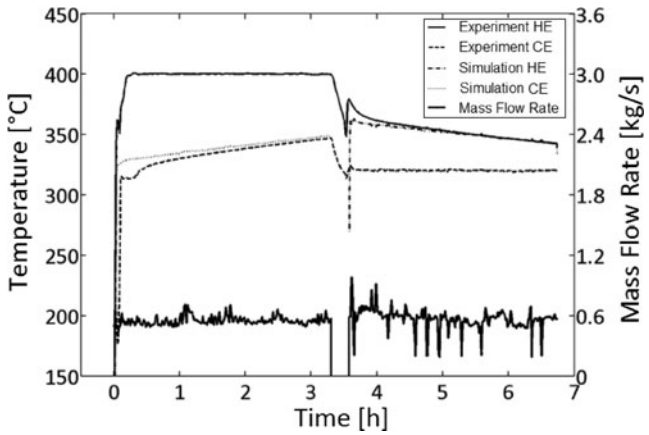

Figure 10 Measured and calculated steam temperatures inside the concrete regenerator.

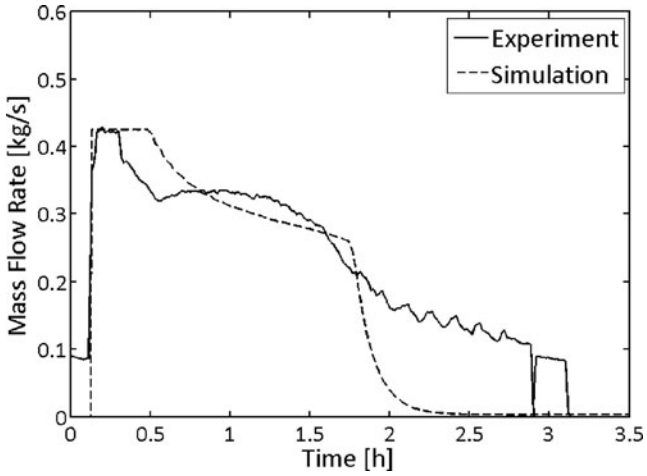

Figure 11 Measured and calculated condensate mass flow rates during charging of the PCM storage.

of 295°C before the cycle was started. The storage material was monitored with several thermocouples distributed over the length and cross section of the storage. The inlet and outlet temperatures of the fluid were monitored by PT100 sensors. The measured data are used as inlet boundary conditions for the simulation.

Figure 11 shows the measured and calculated condensate mass flow rates during charging of the PCM storage. Since the maximum feed flow rate is restricted to 0.425 kg/s by specifics of the test facility, the condensate flow rate is limited at the beginning. The PCM module would allow for even higher rates. In the experiment, this maximum flow rate persists for about 10 min, while the calculated value stays at the maximum for more than 20 min. In both cases, a clear reduction of the condensate mass flow rate occurs. Although the simulated curve declines evenly, the measured curve shows first an increasing condensate rate then decreasing. At time 0.5 h a slight increase follows, but finally the condensate rate decreases after about 1 h. This temporary increase is assumed to originate from convective flows inside the liquid phase of the melting PCM, which may lead to significantly improved heat transfer inside the storage. Although the model is not able to describe this phenomenon, the difference of calculated and measured mass flow rate lies predominantly within the accuracy of the measurement equipment. At time 1.8 h, the simulated condensate flow rate breaks in completely. Subsequently, the measured values show a pulsating behavior. This is an indication that either the condensation process changed or the measurement is erroneous. With regard to the integrated enthalpy flows over 2 h, experiment and calculation both provide a transfer of approximately 800 kWh, which is the maximum capacity of the storage. A possible explanation is that condensation occurs in the piping behind the lower end of the PCM-module, due to high heat losses once the storage is completely charged; therefore, a certain condensate mass flow is still measured.

The measured and calculated mass flow rates of generated steam during discharging are displayed in Figure 12. The

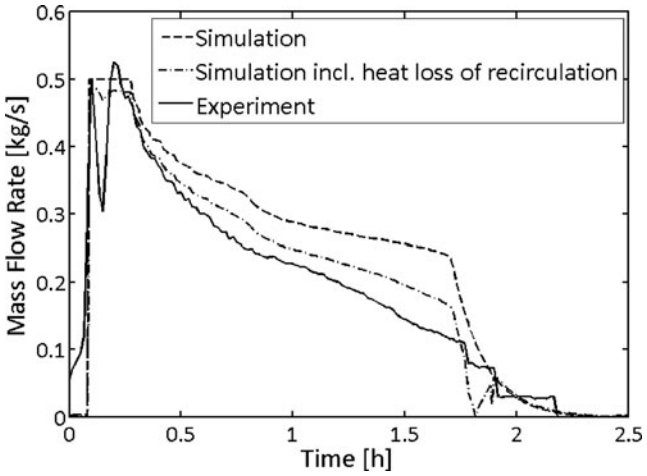

Figure 12 Measured and calculated steam generation during discharging of the PCM storage.

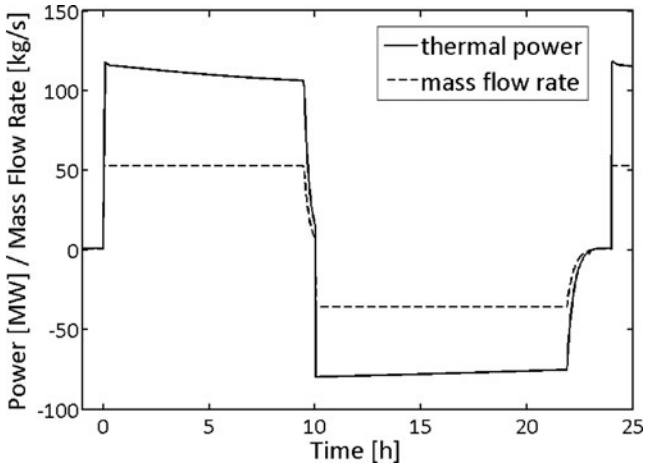

Figure 13 Calculated mass flow rates and thermal power of a 1000-MWh_{th} storage system.

recirculation rate is constant at 0.5 kg/s during the discharging process, limiting the maximum steam mass flow rate at the beginning when the complete feed-water flow is evaporated. After the initial peak, calculated and measured steam mass flow rates decrease continuously due to the increasing thermal resistance of the growing solid salt layer until the storage is fully discharged. With increasing discharging time, the difference between calculated and measured steam mass flow rates increases. While the model predicts that saturated steam with an integrated enthalpy of approximately 750 kWh is produced, the experimental steam release is only about 590 kWh, corresponding to thermal efficiencies of 94% and 74%, respectively. Reasons for this discrepancy are the heat losses occurring in the recirculation piping, the pump, and the steam drum, which were determined to be 25 kW in a separate experiment. After adding this heat loss to the model, the agreement between experiment and simulation is considerably improved. The maximum deviation between simulated and measured mass flow rate, as shown in Figure 12, is reduced from 0.14 kg/s to 0.06 kg/s, supporting the validity of the presented method to calculate the heat transfer during evaporation. The excessive heat losses obtained at the test facility are caused by its specific design. In a future application, the recirculation apparatus must be integrated into the heat storage's thermal insulation to minimize its heat losses.

DESIGN OF A 1000-MWh_{Th} STORAGE SYSTEM

The previously described models are combined into an overall system as shown in Figure 1. The aim of this exercise is to estimate the size and performance of a storage system with a thermal capacity of 1000 MWh_{th}. The design of the storage modules has been performed in an iterative process to maximize the energy densities. The tube dimensions are 21.3 × 3.2 mm for the PCM and 24.5 × 3.2 mm for the concrete module. Heat losses were estimated according to the expected surfaces of the module. The assumed boundary conditions are listed in Table 3.

Table 3 Boundary conditions for the system simulation

Cycle (charging/discharging)	10/14 h
Pressure (charging/discharging)	105.6/80.0 bar
Rated mass flow rate (charging/discharging)	52.8/35.5 kg/s
Steam inlet temperature during charging	500°C
Feed temperature during discharging	260°C

As depicted in Figure 13, the mass flow rate of 52.8 kg/s can be maintained over 9.5 h of charging. The charging mass flow rate decreases when the PCM storage is completely liquid. Due to the increasing temperature of the preheater module, which results in an increasing condensate outlet temperature from about 260 to 300°C (see Figure 14), the total absorbed power decreases from 118 to 106 MW. After shifting to discharge operation, the mass flow rate of 35.5 kg/s is maintained for 12 h. The transmitted power is almost constant, decreasing slightly from 80 to 75

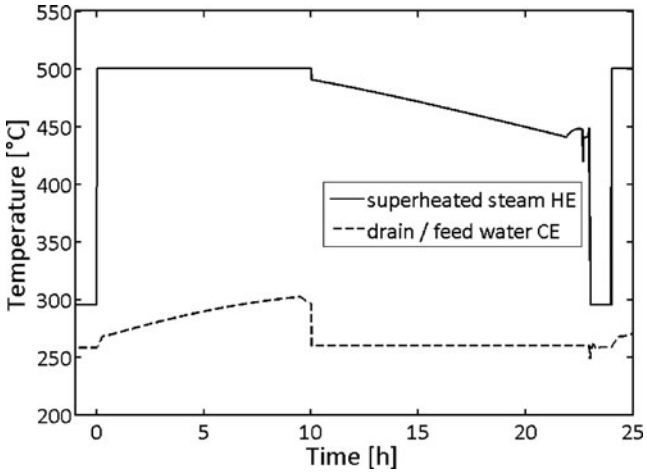

Figure 14 Calculated temperatures at the system boundary of the storage system (hot and cold nozzle).

Table 4 Calculated size of the 1000-MWh_{th} system

Module	No. of tubes	Length (m)	Volume (m^3)	Capacity (MWh)	Specific capacity (kWh/m^3)
Preheater module	2052	89	2845	73	26
Evaporator module	42,000	10	6490	710	109
Superheater module	2052	302,6	9674	297	31

MW. When the system is totally discharged, the steam flow rate and the heat flow rate both decline to zero. Due to the decreasing temperature of the superheater module during discharging, the outlet temperature of the generated superheated steam decreases from 491 to 439°C. In total, this storage system is predicted to absorb 1080 MWh and to provide 940 MWh. This is equivalent to an efficiency of 87%. The capacity distribution of individual several modules and their calculated characteristics are given in Table 4.

Contrary to the experimental procedure with the PCM storage described earlier, the power of the designed storage system is throttled, in order to generate almost constant outlet conditions.

The calculated pressure losses are less than 1 bar for the superheater module. Therefore, acceptable operation would be possible. However, this examination was done for monolithic blocks; a realistic storage system would consist of an arrangement of standard modules that would have to be connected by transfer lines. The resulting layout is unknown at this stage of development. Because of expected variations in cross section and flow direction, considerable pressure losses may occur.

CONCLUSIONS AND OUTLOOK

To describe a coupled modular storage system of PCM and concrete heat storage units, effective models were developed and experimentally validated. For both types of storage, the mass of the storage is approximated by parallel hollow cylinders. For the concrete regenerator, a method was used where the convective heat transfer is adapted to account for the heat conduction inside the storage material, so that the storage mass can radially be treated as a lumped system. In the case of PCM storage, the hollow cylinder is discretized in the radial and the axial directions to find the solution numerically. Single-phase convective heat transfer and two-phase convective heat transfer were described by well-established methods. The functionality of both kinds of thermal storages was experimentally proven. Methods for the thermal description of the concrete regenerator and the PCM storage for direct steam generation were identified and developed. With these models, an iterative dimensioning of single and coupled modules is possible. Heat losses, efficiencies, transmitted power, and system temperatures can be predicted.

In the next stage, the efficiency of the integration of such a system into a real solar thermal power plant has to be demonstrated. Then, detailed engineering of the system, such as the arrangement of the modules and the design of the connectors between the modules, has to be examined.

NOMENCLATURE

A	surface, m^2
A_c	cross-sectional area, m^2
c	specific heat capacity, J/(kg-K)
CE	cold end
f_η	waviness of film factor
f_{well}	temperature-dependent property factor
F	enhancement factor
g	gravitational acceleration
h	specific enthalpy, J/kg
HE	hot end
$\dot{m}$	mass flow rate, kg/s
Nu	Nusselt number
$\dot{Q}$	heat flow rate, W
r	radius, m
S	suppression factor
t	time, s
T	temperature, °C
$\dot{V}$	volumetric flow rate, m^3/s

Greek Symbols

α	heat transfer coefficient, $W/(m^2\text{-}K)$
λ	thermal conductivity, W/(m-K)
ρ	density, kg/m^3
υ	kinematic viscosity, m^2/s

Subscripts

amb	ambient
B	boiling
C	convection
f	fluid
F	film
H	Hausen
i	inner
L	heat loss
l	liquid, laminar
m	melt
o	outer
r	radial
s	storage material, solid
t	turbulent
x	local, axial

REFERENCES

[1] STEM project (Solar Thermal Electricity in the Mediterranean (STEM), EU funded project under reference APAS (RENA-CT94-0014), 1996.

[2] Eck, M., Zarza, E., Eickhoff, M., Rheinländer, J., and Valenzuela, L., Applied Research Concerning the Direct Steam Generation In Parabolic Troughs, *Solar Energy*, vol. 74, issue 4, pp. 341–351, 2003.

[3] Birnbaum, J., Eck, M., Fichtner, M., Hirsch, T., Lehmann, D., and Zimmermann, G., A Direct Steam Generation Solar Power Plant With Integrated Thermal Storage, *Journal of Solar Energy Engineering*, vol. 132, 2010.

[4] Price, H., and Kearney, D., Reducing the Cost of Energy From Parabolic Trough Solar Power Plants, *Proceedings of ISEC 2003*, pp. 16–18, 2003.

[5] Steinmann, W-D., Laing, D., and Tamme, R., Storage Systems for Solar Steam, ISES Solar World Congress, pp. 2736–2740, 2007.

[6] http://www.abengoasolar.es/corp/web/en/our_projects/solucar/ps10/index.html, 01.12.2010.

[7] Beckmann, G., and Gilli, P. V., *Thermal Energy Storage, Basics–Design–Applications to Power Generation and Heat Supply, Springer*, Berlin, Germany, 1984.

[8] Goldstern, W., *Dampfspeicheranlagen: Bau, Berechnung und Betrieb industrieller Wärmespeicher*, Springer, Berlin, Germany, 1963.

[9] Laing, D., Bahl, C., Bauer, T., Lehmann, D., and Steinmann, W.-D., Thermal Energy Storage for Direct Steam Generation, vol. 85, pp. 627–633, 2010.

[10] Laing, D., Bahl, C., Fiß, M., Hempel, M., Meyer-Grünfeldt, M., Eickhoff, M., and Stückle, A., Test and Evaluation of a Thermal Energy Storage System for Direct Steam Generation, SolarPACES, 2011.

[11] Fritzson, P. A., Principles of Object-Oriented Modeling and Simulation With Modelica, Wiley-Interscience, 2004.

[12] Tiller, M., *Introduction to Physical Modeling With Modelica*, Kluwer Academic, Dordrecht, The Netherlands, 2001.

[13] *Dymola Dynamic Modeling Laboratory User Manual,* vol. 1., Dynasim AB (A Dassault Systèmes Company), 2009. Retrieved from http://www.dynasim.se

[14] Laing, D., Bahl, C., Bauer, T., Fiss, M., Breidenbach, N., and Hempel, M., High-Temperature Solid-Media Thermal Energy Storage for Solar Thermal Power Plants, *Proceedings of the IEEE*, 2011.

[15] Gnielinski, V., Heat Transfer in Pipe Flow, in *VDI Heat Atlas*, Springer, Berlin, Germany, Section G1, 2010.

[16] Schmidt, F. W., and Willmott, A. J., Thermal Energy Storage and Regeneration, McGraw-Hill, New York, NY, 1981.

[17] Hausen, H., *Näherungsverfahren zur Berechnung des Wärmeaustausches in Regeneratoren*, 1931. doi: 10.1002/zamm.19310110204

[18] Schack, K., *Der industrielle Wärmeübergang*, Verlag Stahleisen mbH, Düsseldorf, Germany, 1983.

[19] Laing, D., Lehmann, D., Fiß, M., and Bahl, C., Test Results of Concrete Thermal Energy Storage for Parabolic Through Power Plants, *Journal of Solar Engineering*, vol. 131, 2009.

[20] Stückle, A., Modelling of High Temperature Storage Systems for Latent Heat, *Proceedings of the 7th International Modelica Conference*, 2009.

[21] Scheffknecht, G., *Ein Beitrag zur Dynamik des Latentwärmespeichers*, VDI-Verlag, Düsseldorf, Germany, 1988.

[22] Numrich, R., and Müller, J., Filmwise Condensation of Pure Vapors, in *VDI Heat Atlas*, Section J1, Springer, Berlin, Germany, 2010.

[23] Baehr, H. D., and Stephan, K., *Wärme- und Stoffübertragung*, Springer, Berlin, Germany, 2006.

[24] Chen, J. C., Correlation for Boiling Heat Transfer to Saturated Fluids in Convective Flow, pp. 322–329, ACS Publications, Washington, D.C., 1966.

Andreas Stückle is head of the Competence Centre Fluidics and Mechanics of HOERBIGER Automation Technology. From 2007 to 2011 he was a research assistant at the Institute of Technical Thermodynamics of the German Aerospace Center (DLR) in Stuttgart, Germany. He studied mechanical engineering at the University of Stuttgart and at the Norwegian University of Science and Technology (NTNU) in Trondheim, Norway. His research interests were high-temperature heat storage forms, in particular development of numerical modeling strategies of regenerators and latent heat storages for direct steam generation. He is a doctoral candidate at the University of Stuttgart.

Doerte Laing is head of the "Thermal Process Technology" Department at the Institute of Technical Thermodynamics of the German Aerospace Center (DLR) in Stuttgart, Germany. She studied mechanical engineering at the University of Karlsruhe, Germany, and University of Birmingham, UK, and has been working in high-temperature solar thermal technology since 1987. Since 2000, she has specialized in thermal energy storage development for applications in solar thermal power plants and industrial process heat.

Hans Müller-Steinhagen is the Rector of Dresden University of Technology, Germany. Previously, he has been director of the Institute of Technical Thermodynamics of the German Aerospace Center (DLR) and of the Institute of Thermodynamics and Thermal Engineering of the University of Stuttgart. His research work covers a wide range of topics related to heat and mass transfer, multiphase flow, fuel cells, solar technologies, and process thermodynamics. He is the author of more than 600 articles and has received numerous international awards, including the 2009 AIChE D. Q. Kern Award. Professor Müller-Steinhagen is a fellow of the Royal Academy of Engineering, past president of EUROTHERM, and chairman of the Advisory Board of the Desertec Industry Initiative.